Nasal airflow simulations suggest convergent adaptation in Neanderthals and modern humans

S. de Azevedo[a,1], M. F. González[a,1], C. Cintas[a,1], V. Ramallo[a], M. Quinto-Sánchez[b], F. Márquez[c], T. Hünemeier[d], C. Paschetta[a], A. Ruderman[a], P. Navarro[a], B. A. Pazos[a], C. C. Silva de Cerqueira[e], O. Velan[f], F. Ramírez-Rozzi[g], N. Calvo[h], H. G. Castro[i,j], R. R. Paz[j,k,2], and R. González-José[a,2]

[a]Instituto Patagónico de Ciencias Sociales y Humanas, Centro Nacional Patagónico, Consejo Nacional de Investigaciones Científicas y Técnicas, U9120ACD, Puerto Madryn, Argentina; [b]Ciencia Forense, Facultad de Medicina, Circuito de la Investigación Científica s/n, Ciudad Universitaria, Universidad Nacional Autónoma de México, Del. Coyoacán, CP 04510, Mexico; [c]Instituto de Biología de Organismos Marinos, Centro Nacional Patagónico, Consejo Nacional de Investigaciones Científicas y Técnicas, U9120ACD, Puerto Madryn, Argentina; [d]Departamento de Genética e Biologia Evolutiva, Cidade Universitária, University of São Paulo, 05508-900, São Paulo, Brazil; [e]Superintendência da Polícia Técnico-Científica do Estado de São Paulo, Equipe de Perícias Criminalísticas de Ourinhos, 19901-560, São Paulo, Brazil; [f]Departamento Académico de Ciencias Morfológicas, Hospital Italiano, C1199ABB, Buenos Aires, Argentina; [g]UMR 5288 Anthropologie Moléculaire et Imagerie de Synthèse, CNRS, 92120 Montrouge, France; [h]Department of Computing, Universidad Nacional del Litoral, S3000, Santa Fe, Argentina; [i]Instituto de Modelado e Innovación Tecnológica, Universidad Nacional del Nordeste, CP W3404AAS, Corrientes, Argentina; [j]Consejo Nacional de Investigaciones Científicas y Técnicas, C1425FQB, Buenos Aires, Argentina; and [k]Livermore Software Technology Corporation, Livermore, CA 94551

Both modern humans (MHs) and Neanderthals successfully settled across western Eurasian cold-climate landscapes. Among the many adaptations considered as essential to survival in such landscapes, changes in the nasal morphology and/or function aimed to humidify and warm the air before it reaches the lungs are of key importance. Unfortunately, the lack of soft-tissue evidence in the fossil record turns difficult any comparative study of respiratory performance. Here, we reconstruct the internal nasal cavity of a Neanderthal plus two representatives of climatically divergent MH populations (southwestern Europeans and northeastern Asians). The reconstruction includes mucosa distribution enabling a realistic simulation of the breathing cycle in different climatic conditions via computational fluid dynamics. Striking across-specimens differences in fluid residence times affecting humidification and warming performance at the anterior tract were found under cold/dry climate simulations. Specifically, the Asian model achieves a rapid air conditioning, followed by the Neanderthals, whereas the European model attains a proper conditioning only around the medium-posterior tract. In addition, quantitative-genetic evolutionary analyses of nasal morphology provided signals of stabilizing selection for MH populations, with the removal of Arctic populations turning covariation patterns compatible with evolution by genetic drift. Both results indicate that, departing from important craniofacial differences existing among Neanderthals and MHs, an advantageous species-specific respiratory performance in cold climates may have occurred in both species. Fluid dynamics and evolutionary biology independently provided evidence of nasal evolution, suggesting that adaptive explanations regarding complex functional phenotypes require interdisciplinary approaches aimed to quantify both performance and evolutionary signals on covariation patterns.

nasal morphology | computational fluid dynamics | quantitative genetics | Neanderthal | *Homo sapiens*

Comparative analysis of osseous structures is at the core of extensive research aimed to infer past microevolutionary and macroevolutionary events in many clades, including Hominins (1, 2). In this context, adaptation to cold climates experienced by some primates, but noticeably Neanderthals and some modern human (MH) populations, have been the focus of qualitative and quantitative analyses of craniofacial and postcranial remains (3–7). Neanderthals have long been described as cold adapted, since they successfully inhabited the cold, dry Eurasian environments from the later Middle Pleistocene to the earlier Late Pleistocene (8). Similarly, northeastern Asian and Arctic MH populations have been identified as carrying a suite of derived traits related to cold adaptations that likely evolved during their spread across

high-latitude Eurasian landscapes (9). Both Neanderthals and some MH populations exhibit narrow superior internal nasal dimensions, a trait that has been postulated as adaptive due to the greater turbulence that it would confer to the nasal airflow (6, 10, 11). However, important Neanderthal-MH differences on craniofacial morphology, including size and shape of the osseous external and internal nose, raise the question whether both species evolved nasal tracts adapted to cold and dry climates on a species-specific manner (8). Indeed, the Neanderthal internal nose presents a set of autapomorphic traits that, overall, may reflect a distinctive species-specific adaptation to cold that differed from the respiratory adaptations exhibited by MHs (3, 7, 8). Although previous research on temperature-sensitive bone growth is focused on endochondral processes (12) that do not include nasal bones development, the experiments made by Mawdsley and Harrison (13) on transplanted bones open the possibility that temperature-sensitive

Significance

Due to its role in humidifying and warming the air before it reaches the lungs, adaptations in the internal nasal anatomy are suspected to have been essential for modern humans and Neanderthals during the settlement of Eurasian harsh landscapes. Unfortunately, the lack of soft-tissue evidence in the fossil record precludes any study of Neanderthal respiratory performance. Here, we use warping techniques to reconstruct a generic Neanderthal nose, computational fluid dynamics simulations to compare the respiratory performance on both species, and evolutionary analyses to detect signals of selection. We report striking differences on fluid residence times under cold/dry climatic conditions. Different from previously suggested, our results indicate that both species would have achieved an advantageous species-specific respiratory performance in cold climates.

cartilage replacement can be a developmental process affecting turbinates' growth. In consequence, temperature-sensitive cartilage growth can be assumed as a phenotypic plasticity process deriving in genetic accommodation as a source of novel nasal traits (14). Given that facial growth involves integrated signaling between all of its hard tissues, be they membranous or endochondral, it is likely that any response to temperature by the ethmoid, which is a cartilage replacement bone, will have an effect on the dimensions and morphology of the nasal airway. Most of the studies on the adaptive significance of Hominin nasal morphology have been concentrated on the size and shape of the skeletal nasal aperture, with few studies focused on the internal nasal anatomy (6, 11, 15–17). Considering that humidity and temperature exchange mainly occurs at the nasal mucosa (18–20), it becomes clear that osseous remains alone are not sufficient to analyze potential differences on the more fragile branching turbinates and the large mucosal area that constitutes the internal nasal tract. Here, we aim to circumvent this problem by reconstructing and analyzing the internal nasal morphology of MHs and Neanderthals, including its mucosa surface, to compare the performance among the Neanderthal nasal model and MHs from two different climates/populations. Then, we simulate the respiratory cycle under several conditions using computational fluid dynamics (CFD) methods (21, 22). To complement this performance approach from a model-bound evolutionary perspective, we test if nasal variation on different clades containing species inhabiting in cold climates is compatible with neutral versus nonneutral evolution. This twofold approach resembles previous works in the larger field of evolutionary biology (23, 24) and biological anthropology (25) that explicitly used mixed datasets with different variables and samples to evaluate adaptive processes from the performance and evolutionary analyses perspectives.

Results and Discussion

Analysis of MH Noses and Reconstruction of Neanderthal Soft Tissues.
We first performed a geometric morphometric analysis (26) on a composite sample including facial computed tomography (CT) scans from 38 representatives of two populations: admixed Argentinians of southwestern European origin (SWE; mainly of Spanish or Italian descent) and northeastern Asians (NEA; Chinese and Korean) migrants in Buenos Aires (*Materials and Methods*), plus the CT scans corresponding to La Ferrassie (LF) and La Chapelle-aux-Saints (LC) specimens, the most complete Neanderthals skulls regarding nasal morphology, enabling the placement of anatomical landmarks in the osseous nasal tract (*SI Appendix,* Table S1). This geometric morphometric analysis thus provides a vector of shape changes representing the main differences between MH and Neanderthal bone nasal morphology (Fig. 1). Next, two MH specimens were chosen as representatives of the SWE and NEA subsamples assumed to have been evolved on temperate and cold climates, respectively, and a 3D mesh/model was obtained for both individuals comprising all of the aspects of soft anatomy, including the external cartilage nose, the internal mucosa surface, and the nasopharyngeal cavity (*SI Appendix,* Fig. S1). Finally, the 3D model corresponding to the average Neanderthal internal nasal morphology (including soft parts) was inferred by warping (26) the SWE model on the vector of SWE-Neanderthal shape changes described in Fig. 1 (*Materials and Methods* and *SI Appendix,* Fig. S1). Although complete nasal tracts are absent from the Neanderthal fossil record, the interpolation approach is valid since we verified that the 3D relationship between the anterior, medial, and posterior landmarks within the nasal cavity covary on a significant and regular pattern across several primate models (*SI Appendix,* Figs. S2–S5 and Tables S2 and S3). Furthermore, we obtained significant covariation patterns among soft and bony landmarks in the modern humans sample at the anterior and posterior planes, further supporting the interpolation method explained above (*SI Appendix,* Fig. S6–S8). The three resulting models are presented in Fig. 2 and were used to develop a description of the nasal physics based on a multiphase CFD model
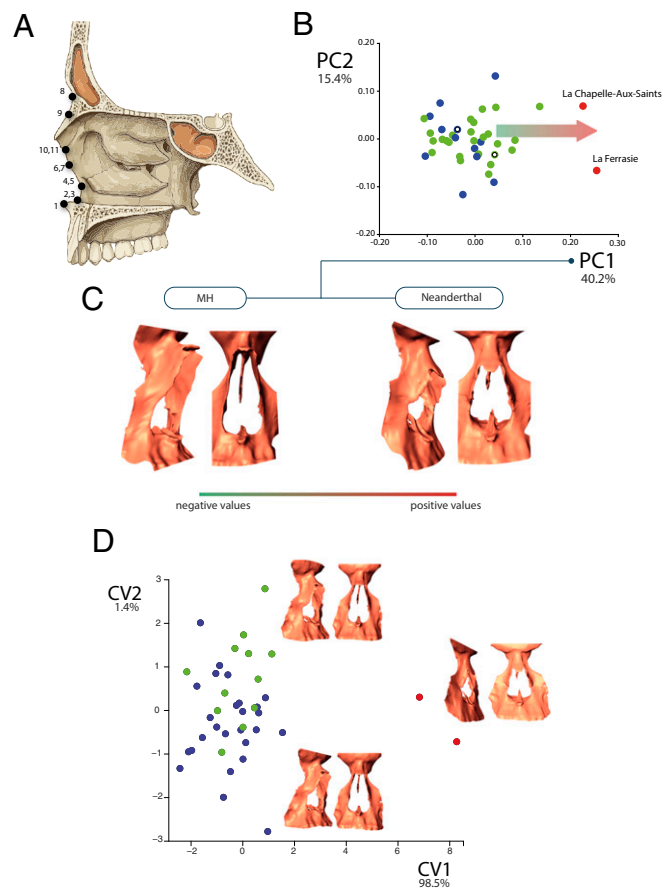

Fig. 1. Nasal morphological variation between MHs and Neanderthals as seen by principal component analysis and canonical variate analysis. (*A*) Scheme representing the anatomical landmarks placed on the external and internal osseous nasal structures (*SI Appendix,* Table S1). (*B*) First two PCs of shape change. NEA, blue dots; Neanderthals, red dots; SWE, green dots. SWE-93776 and NEA-2116236 specimens are indicated with empty dots. The arrow represents the displacement across the morphospace used to obtain the Neanderthal soft anatomy departing from the MH internal cavity, including the mucosa and turbinate soft structures. (*C*) Internal nasal cavity warped shape changes occurring across the first PC. The shape change defining the MH nose involve a general narrowing of the nose, both in their superior and inferior parts, along with an anterior-posterior alignment of the most anterior part of the concha with the external nasal border. The Neanderthal anatomy, conversely, is characterized by broader noses in general, along with a deflection of the anterior limit of the concha, which is placed on a more medial position in relation to the external border of the nose. In addition, an inspection on the sagittal plane of these shape changes indicate that MH noses present a more anterior projection of the medial part of the nasal border, whereas Neanderthals present, in general, a more flat nasal plane. (*D*) First and second canonical axes obtained from the first five PCs depicting shape changes that most differentiate the three groups (Neanderthals, SWE, NEA) in terms of nasal shape. The centroid shape of each group is presented as a warped internal nose. Discriminant functions among the three groups, with P values obtained after 10,000 permutations are as follows: SWE-Neanderthal Mahalanobis distance: 11.5 ($P = 0.006$). NEA-Neanderthal Mahalanobis distance: 55.3 ($P = 0.029$). SWE-NEA Mahalanobis distance: 2.48 ($P = 0.005$).

for mass, momentum, and energy transport of an in-compressible viscous fluid mixture: air and water vapor. The model was run after different parameters of external temperature and humidity climatic conditions to simulate warm-humid versus cold-dry climates (27), and to evaluate whether MHs and/or Neanderthal nasal cavities show features that tend to improve the mucosa/air contact for an effective air conditioning. Simulations of inspiratory and expiratory movements were developed under both basal conditions and exercise regimes (*SI Appendix*).
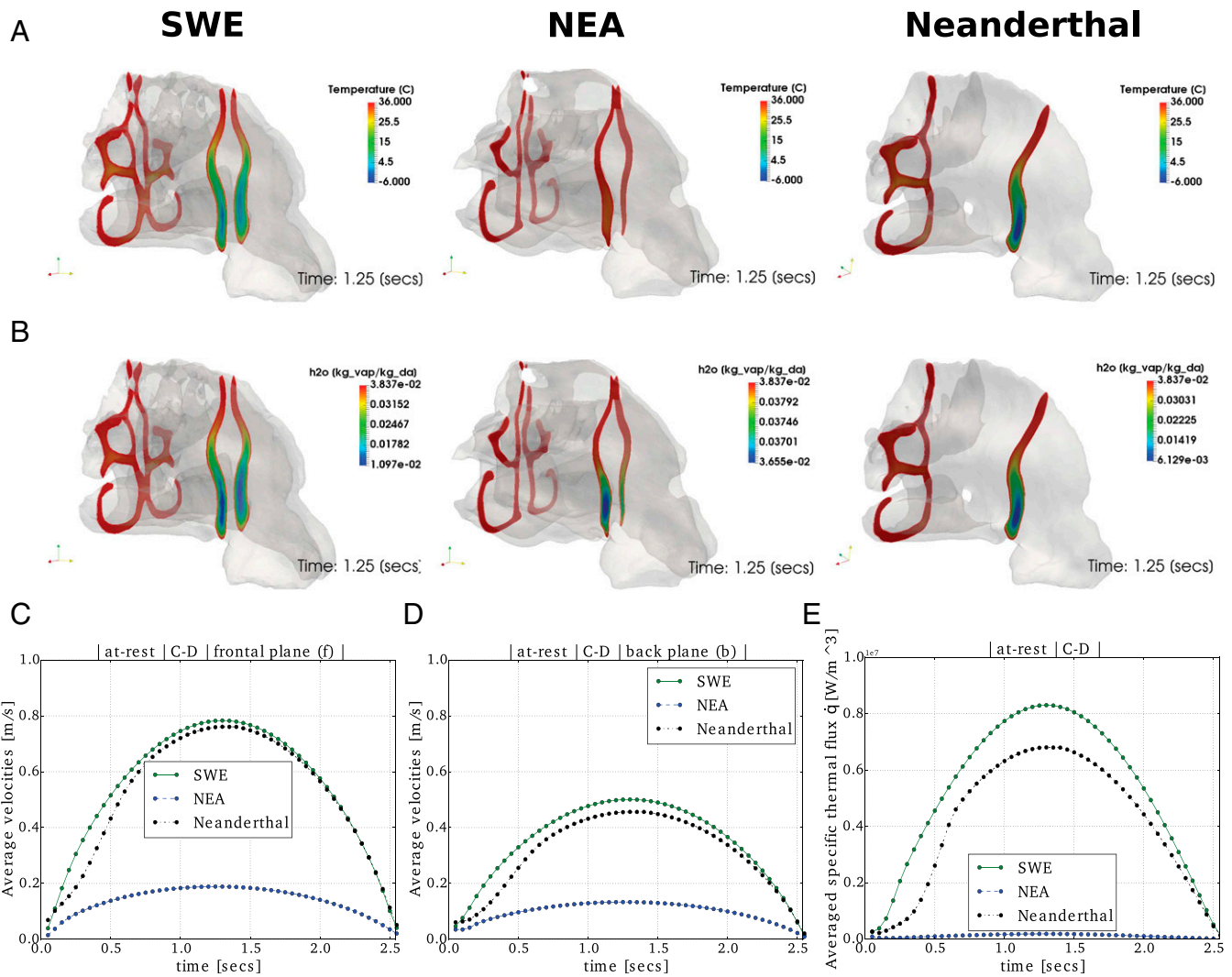
Fig. 2. CFD model results. Temperature (°C) (*A*) and specific humidity [kg$_{vap}$/kg$_{da}$]) fields (*B*), at rest for forward (f: nasal vestibular zone) and backward (b: nasopharyngeal tract zone) planes when the pressure drop is maximum (*t* = 1.25 s; *SI Appendix*, Eq. S8) in cold-dry weather conditions for SWE, NEA, and Neanderthal. The temperature distribution in frontal planes f, when the breathing cycle reaches a maximum flow rate, shows that the mixture achieves the conditioning temperature faster for the NEA specimen, followed by Neanderthals showing an intermediate performance, especially in the superior part of the tract, and then by SWE, showing a relative worst performance. The temperature close to the oropharynx (plane b) is totally conditioned in NEA cavity and almost fully conditioned for the other two cavities. The moisture content or specific humidity at frontal planes follows the same behavior as the temperature field, being bigger in average for NEA nose, followed by Neanderthals and SWE. Specific humidity is in full saturation in plane b for NEA and almost saturated for Neanderthal and SWE noses. Averaged velocities at planes f and b are shown in *C* and *D*, respectively. It can be observed that the magnitude of the established velocities is 3.5–4 times bigger in the SWE and Neanderthal cavities than in NEA. Then, the residence time of a volume of mixture will be longer in NEA than in SWE and Neanderthals, enhancing the heat transfer from mucosa to the fluid and consequently the moist conditioning. *E* shows the volume-averaged specific thermal flux $q = u_{avrg}\rho c_p (T_{wall} - T_{mix}) A_{nose}/V_{nose}$ (in [W/m^2]) needed for the conditioning of each specimen. u_{avrg} is the average of the velocity field using data of *C* and *D*, and A_{nose} and V_{nose} are the mucosa surface area and nose volume (*SI Appendix*), respectively. See *SI Appendix*, Figs. S9 and S10 for further details.

Respiratory Performance on MHs and Neanderthals. CFD main results (Fig. 2; *SI Appendix*, Figs. S9 and S10; and Movies S1–S12) indicate that in the three models under analysis, variations in the shape of the nasal cavity are related to gradual changes from cold-dry to warm-humid climates, with separate effects on temperature and water vapor. Furthermore, it is verified that a significant portion of the thermal conditioning is attained at the level of the nasal vestibular region, before reaching the nasopharyngeal tract, as previous climate/nasal shape covariation studies suggested (6). Some recurrent patterns can be observed across the three specimens. For instance, none of them present problems to achieve optimal air-conditioning on simulated warm, humid climates (*SI Appendix*, Figs. S9 and S10). Also, air conditioning patterns observed under basal metabolic conditions

(at rest) are similar to those obtained under an exercise regime (*SI Appendix*, Figs. S9 and S10). In general terms, all of the simulations indicate that, despite the specimen considered or the climatic conditions simulated, low SDs in temperature and humidity values show that the inspired air is fully conditioned when arriving to the posterior nasal tract. This shows the importance of the most-anterior part of the nose as a central structure for humidity and temperature exchange (6). However, when simulating the performance of the anterior tract, the NEA model achieves faster air uniformity, followed by Neanderthals, which is an expected result considering that the residence time is close to three times greater in NEA in relation to Neanderthals and SWE. This suggests that the general craniofacial shape divergence, including a significant facial flattening, that occurred

de Azevedo et al.

during the settlement of northeastern Asia by MHs, could be correlated to anatomical changes that enhance the respiratory function via variation in residence time.

Evolutionary Analyses: The Lande's Gene-Drift Test. As a complementary analysis, we implement the Lande's gene-drift test (1, 28, 29), aimed to test for signals of genetic drift, stabilizing selection, or diversifying selection by comparing the proportionality of among-population to within-population variances (*Materials and Methods*). To this purpose, we used 3D landmark coordinates placed on craniofacial (including nasal) structures (*SI Appendix*, Table S4) in a sample of 255 skulls belonging to 11 MH populations from different climates, *Macaca* spp. monkeys including a cold-adapted species (*Macaca fuscata*, at least in relation to the climate conditions of the clade's common ancestor), and a composite sample of Hominins including *Australopithecus*, *Paranthropus*, and *Homo* genera (*SI Appendix*, Table S5). This dataset provides a phylogenetic context where some members of a clade evolved in cold climates whereas others do not (Fig. 3), thus maximizing the chances of detecting potential nonstochastic signals not due to across-clades spurious comparisons (see refs. 10, 30, and 31). Lande's test predicts that, under a scenario of evolutionary divergence driven exclusively by stochastic factors, among-population variation

should be proportional to within-population variation (1, 28, 29). Results presented in Table 1 and Fig. 3 suggest that, whereas the covariation patterns of the skull as a whole are compatible with evolution under stabilizing selection, the nasal structures seem to have evolved mainly by stochastic forces. However, on a population level, MH noses show a signal of stabilizing selection that, interestingly, turns into compatible with neutral evolution when Arctic populations (Inuit) are removed from the analysis (*SI Appendix*, Table S6). This suggests that specific, derived nasal traits are necessary to explain the morphology of humans occupying cold environments under a scenario of stabilizing selection. Furthermore, a composite MH–Neanderthal analysis provided results compatible with stochastic nasal evolution (*Materials and Methods* and Table 1), further suggesting that adaptive changes in terms of osseous nasal tracts seems to have occurred only in human groups inhabiting Arctic environments.

Both the "mechanistic" CFD approach and the comparative evolutionary analysis independently and complementary test the hypothesis that some MH populations and/or Neanderthals experienced complex changes in soft and hard tissues of the nasal tract compatible with adaptation to cold climates. Note that, since environmentally induced variants such as potential temperature-sensitive modifications in the turbinates growth and development are heritable as well (14), the Lande's test of neutral evolution is still useful to infer the evolutionary potential of the nasal tract, no matter which genetic and developmental factors interact to influence the observed phenotypic variability.

Our twofold approach agrees with previous statements (3, 4, 7, 30) indicating that *Homo neanderthalensis* do not present a nasal phenotype compatible with adaptation to cold climates, at least in osteological terms. In addition, a comparison of PAX3 SNPs frequencies associated to nasion position (32) in MH populations and Neanderthal genomes (*SI Appendix*, Table S7) indicates that the latter share both the genetic background of high nasal tracts present in Europeans along with PAX3 variants associated to broad noses.

Conclusions

Neanderthals are autoapomorphic in cranial terms including nasal hard tissues (7), although this condition along with stochasticity defining MH–Neanderthal divergence (4) (Table 1), did not inhibit their reconstructed nasal mucosa from performing well under cold and dry simulated conditions. In consequence, stabilizing selection at the whole craniofacial complex can be seen as a constraint to faster nasal change during the evolution of our clade. The exception to this pattern appears to be in the nasal shape of peri-Arctic groups that seem to achieve both conditions: The NEA nose performs better in cold-dry climates, and the removal of flattened-face populations (Inuit) from evolutionary analyses turn covariance patterns compatible with stochastic evolution. In other words, a nasal performance suitable with living in cold and dry environments can be seen as a case of convergent adaptation involving both MH Arctic populations and Neanderthals. This reinforces the notion that the human face is a complex phenotype, where integration and modularity patterns operate at different layers of the genotype-phenotype map (33, 34), including genetic, developmental, and phenotypic plasticity variation driving evolution and adaptation to novel environments.

Materials and Methods

Geometric Morphometrics of Modern Human and Neanderthal Nasal Cavities. We analyzed a sample of facial CT scans of 38 MHs collected at the Hospital Italiano Image Service during three recruitment episodes in 2010, 2011, and 2012. Scans were obtained using both the Toshiba Aquilion 16 and Toshiba Aquilion 64 facilities belonging to the Hospital Italiano. Individuals were recruited during its visit to the service as part of diagnosis trials of pathologies or trauma not related to the external or internal nose. After signing of the
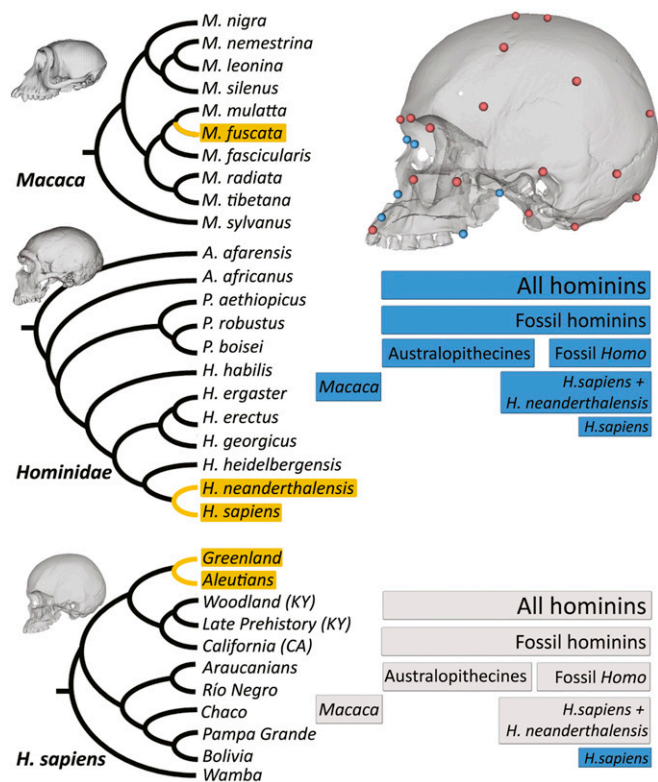

Fig. 3. Phylogenetic framework and results for Lande's genetic drift test. (*Left*) Cladograms depicting the position of cold-adapted species/populations (in terms of the ancestral climate condition, shown in yellow branches and boxes) in Macaca (*Top*), Hominidae (*Middle*), and *Homo sapiens* (*Bottom*) clades. Further details on samples characteristics can be found in *SI Appendix*, Table S5. See refs. 10, 30, and 31 for further discussion on this topic. (*Right Top*) Whole skull configuration (all dots) and nasal configuration (blue dots). (*Right Middle* and *Right Bottom*) Lande's results for the hierarchical groups studied here: all hominins, *H. sapiens* populations, fossil hominins, *Macaca* genus, fossil *Homo* species, Australopithecines, *H. sapiens* + *H. neanderthalensis*, whole skull configuration (*Middle* scheme) and nasal configuration (*Bottom* scheme). Blue boxes, Lande's results compatible with stabilizing selection operating at the taxonomic level under study; gray boxes, Lande's results compatible with genetic drift.

ANTHROPOLOGY

Table 1. Lande's genetic drift results

Taxa	n	Evolutionary outcome	Slope	Low	Sup	R² adj	P
Shape Space: Whole skull							
Macaca	10	GD	1.12	0.97	1.28	0.87	0.1207
All homininis	22	SS	0.46	0.33	0.59	0.41	0.0000
Homo sapiens	11	SS	0.84	0.74	0.94	0.80	0.0023
Fossil hominins	11	SS	0.56	0.46	0.67	0.64	0.0000
Fossil *homo*	6	SS	0.55	0.44	0.67	0.57	0.0000
Australopithecines	5	SS	0.51	0.38	0.63	0.50	0.0000
H. sapiens-H. neanderthalensis	12	SS	0.58	0.41	0.75	0.40	0.0000
Shape Space: Nasal							
Macaca	10	GD	0.99	0.78	1.19	0.92	0.91
All hominins	22	GD	1.01	0.35	1.68	0.52	0.97
H. sapiens	11	SS	0.58	0.37	0.79	0.79	0.00
Fossil hominins	11	GD	1.19	0.61	1.77	0.67	0.48
Fossil *homo*	6	GD	1.16	0.52	1.80	0.61	0.58
Australopithecines	5	GD	1.15	0.59	1.71	0.67	0.56
H. sapiens-H. neanderthalensis	12	GD	0.81	0.29	1.32	0.53	0.43

Regression of between-group on within-group variances as a test for genetic drift. Estimation of regression slopes, lower and upper 95% confidence intervals (Low, Sup), and P values associated to the null hypothesis of neutral evolution ($\beta = 1$) are shown. n, number of species/populations included in the analysis. R^2 adj, adjusted R squared for the regression test. The estimated evolutionary outcome (GD, genetic drift; SS, stabilizing selection) are also shown, according to the regression slope values (GD: $b = 1$, SS: $b < 1$, respectively; see *Methods* for details). The hierarchical level of analysis corresponds to the scheme depicted in Fig. 3. Note for instance that "All hominins" level includes *Australopithecus*, *Paranthropus*, and *Homo* genera, including *H. sapiens*.

informed consent approved by the ethics committee of the Hospital Italiano (Enmienda I, October 17, 2010), patients were submitted to a survey regarding their population origins, drug/medicine consumption, and medical antecedents of superior nasal tract pathologies. Population origin was derived after asking for the born place of parents, grandparents, and great grandparents. Due to the recent increase of the Chinese migrant community in Buenos Aires, this survey enabled us to separate the sample into two marked and clear-cut groups: one of admixed Argentineans of southwestern European (mainly Spanish and Italian) origin ($n = 26$), and another of recent (first- or second-generation) Chinese migrants in Buenos Aires ($n = 12$; see *SI Appendix*). Craniofacial differences among northeastern Asians and southwestern Europeans were reported elsewhere (9, 35), thus guaranteeing a great deal of modern human craniofacial variation involving cold-adapted (northeastern Asians) versus temperate warm-adapted (southwestern Europeans) populations. Additionally, CT scans taken on two classic Neanderthal specimens, La Ferrassie and La Chapelle-aux-Saints, were included in the sample. Both specimens were selected among many Neanderthal remains because they offer the largest conservation of the internal bony structure of the nose (36), thus providing a minimal osseous "template" against which to extrapolate the modern human mucosa coverage (see below). CT scans were explored using the 3D Slicer software (v 4.1.0; https://www.slicer.org) to place a 3D configuration of 11 landmarks (*SI Appendix*, Table S1) located exclusively on the osseous tissue (Fig. 1 and *SI Appendix*, Fig. S1). Even when landmark coverage in both external and internal nasal structures is limited by the conservation state in both Neanderthal specimens, this landmark configuration enables a proper coverage of the lateral walls, the roof top, the floor, and the nasal concha in all of the 38 + 2 analyzed specimens. To analyze the main morphological trends in the sample, we computed a principal component analysis and a canonical variate analysis using MorphoJ (37). As expected, the resulting morphospace is occupied by the two Neanderthals specimens in the positive values of the first PC, whereas the MH samples occupy the negative region of the morphospace defined by the two first PCs, explaining 54.6% of the total nasal variance (Fig. 1). The morphospace resulting of this PCA depict the main differences in the osseous nasal structures separating Neanderthals from MHs (Fig. 1), and were used as the raw data to reconstruct the extension of the mucosa on the extinct species as a preliminary step to perform the CFD respiratory simulations. To do so, we first selected two individuals from the living MH facial CT scans subsample (Fig. 1). Both individuals were chosen as representatives of their populations (southwestern European versus northeastern Asian ancestry).

Reconstruction of the Internal Nasal Cavities in MHs. We used a minimum of 140 sections from the CT images of both subjects to construct an anatomically correct 3D model of the nasal and pharyngeal cavities. The images were

obtained at intervals of 1 mm from the plane delimited by the nasal apertures to the posterior end of the pharynx, at the level of the posterior nasal spine. The 3D geometry of the nasal and pharyngeal cavities including the mucosa extension was reconstructed based on the DICOM (digital imaging and communications in medicine) data of the CT scan sections by using the imaging software 3D Slicer (https://www.slicer.org). The CT scans belonging to both specimens were segmented by manual outlining of the nasal boundaries on successive images to yield a surface triangulation for each image dataset. The data subset selected into 3D slicer was further exported to meshlab code (www.meshlab.net/) to make a starting boundary mesh. Although this mesh is useful for geometry visualization purposes, it is inadequate for CFD analysis. The last steps on mesh-healing, triangle-shape optimization, adapting density to the CFD requirements, discrimination of surfaces with different boundary condition (for the calculus stage), and filling the volume with shape-and density-controlled tetrahedra, was made on Meshsuite (38), adapted ad hoc for this kind of domain and the meshes. After necessary smoothing and artifact correction, the resulting average mesh size is $h = 1.3 \times 10^{-4}$ m for both specimens. The meshes representing the nasal cavity for the southwestern Europeans and northeastern Asian models with different levels of refinement ranged from 50,000 to 240,000 nodal points, giving differences of 1–2% in the variables between the coarser and the finer mesh. CFD simulations were run on both domains according to the conditions explained below.

Reconstruction of the Internal Nasal Cavities in Neanderthals. Since our ultimate goal is to compare the performance of the nasal cavity between humans and Neanderthals, we used warping techniques (26, 39) to infer the extension of the soft tissues into the Neanderthal cavity (the unknown target shape), departing from extrapolating the relationship between mucosa and bony structures observed in humans (an observed reference shape) to the bony structure observed in Neanderthals (an observed target shape). Specifically, we first performed an orthogonal projection of the landmarks placed on the osseous tissue (*SI Appendix*, Fig. S1) to the surface of the mucosa represented in the mesh obtained as explained above. This represents the geometric soft counterpart of the osseous nasal cavity that respects the real extension of the mucosa into the nasal cavity. Thus, taking the southwestern European nasal cavity surface as the starting shape, we used Landmark software (40) to warp the surface using the vector of European-average Neanderthal shape changes imported previously from MorphoJ (see above). Note that, in relation to the placement of Neanderthals on the morphospace, the SWE-NEA difference has no significant effects on the selection of SWE or NEA as the starting shape (Fig. 1). Since the right side of the Neanderthal specimens is best preserved than the left one, we inferred just the right side of the Neanderthal internal nasal anatomy. The resulting

de Azevedo et al.

mesh representing the 3D Neanderthal geometry consist of 350,000 cells and 80,000 nodal points and, to the best of our knowledge, takes the best amount of biological information regarding *H. neanderthalensis* remains to achieve an approximation to the true, anatomically functional internal nasal geometry of this extinct species. The two reconstructed nasal cavities of the individuals of southwestern Europeans and northeastern Asian ancestry, together with the estimated nasal cavity shape for Neanderthals, were used in further analyses to simulate the respiratory cycle under different climatic conditions. See *SI Appendix*.

Quantitative Genetic Models: The Lande's Test of Genetic Drift. Quantitative genetic models yield specific predictions about the relationship linking within- and between-population variation patterns. The relationship between both levels of variation can be used to test the null hypothesis of neutral evolution, instead of assuming that all morphological variation is adaptive. An assumption of neutrality is a useful starting point even if incorrect because providing unambiguous, testable predictions allows detecting deviations of the null hypothesis of neutral evolution by examining the expected magnitudes and patterns of shape divergence under the influence of genetic drift and mutations alone (1, 28, 29). Here, we employ the β-test presented in references (1, 26), which is based on quantitative-genetic theory (28) aimed to test for signals of genetic drift by comparing the proportionality of among- to within-population variances using geometric morphometric data. This approach is based on the notion that evolutionary mechanisms depend on intraspecific variation as a fuel for population diversification, and therefore morphological change through time is rooted in an understanding of population level variation and covariation (28). Considering that evolutionary theory predicts a proportional relationship linking within- to between-group phenotypic variation if populations have diversified through random evolutionary processes such as genetic drift and mutations alone, the β-test uses a simple regression of between-group variances (B) on within-group variances (W) across shape variables to test the proportionality of (B and W) variances (1, 29). See *SI Appendix*.

1. Ackermann RR, Cheverud JM (2004) Detecting genetic drift versus selection in human evolution. *Proc Natl Acad Sci USA* 101:17946–17951.
2. Martínez-Abadías N, et al. (2012) Pervasive genetic integration directs the evolution of human skull shape. *Evolution* 66:1010–1023.
3. Franciscus RG (2003) Internal nasal floor configuration in Homo with special reference to the evolution of Neandertal facial form. *J Hum Evol* 44:701–729.
4. Weaver TD, Roseman CC, Stringer CB (2007) Were neandertal and modern human cranial differences produced by natural selection or genetic drift? *J Hum Evol* 53:135–145.
5. Savell KRR, Auerbach BM, Roseman CC (2016) Constraint, natural selection, and the evolution of human body form. *Proc Natl Acad Sci USA* 113:9492–9497.
6. Maddux SD, Butaric LN, Yokley TR, Franciscus RG (2017) Ecogeographic variation across morphofunctional units of the human nose. *Am J Phys Anthropol* 162:103–119.
7. Franciscus RG (1999) Neandertal nasal structures and upper respiratory tract "specialization". *Proc Natl Acad Sci USA* 96:1805–1809.
8. Márquez S, Pagano AS, Delson E, Lawson W, Laitman JT (2014) The nasal complex of Neanderthals: An entry portal to their place in human ancestry. *Anat Rec (Hoboken)* 297:2121–2137.
9. Roseman CC (2004) Detecting interregionally diversifying natural selection on modern human cranial form by using matched molecular and morphometric data. *Proc Natl Acad Sci USA* 101:12824–12829.
10. Holton NE, Yokley TR, Franciscus RG (2011) Climatic adaptation and Neandertal facial evolution: A comment on Rae et al. (2011). *J Hum Evol* 61:624–627, author reply 628–629.
11. Fukase H, Ito T, Ishida H (2016) Geographic variation in nasal cavity form among three human groups from the Japanese Archipelago: Ecogeographic and functional implications. *Am J Hum Biol* 28:343–351.
12. Serrat MA (2014) Environmental temperature impact on bone and cartilage growth. *Compr Physiol* 4:621–655.
13. Mawdsley R, Harrison GA (1963) Environmental factors determining the growth and development of whole bone transplants. *J Embryol Exp Morphol* 11:537–547.
14. West-Eberhard MJ (2005) Developmental plasticity and the origin of species differences. *Proc Natl Acad Sci USA* 102:6543–6549.
15. Evteev A, Cardini AL, Morozova I, O'Higgins P (2014) Extreme climate, rather than population history, explains mid-facial morphology of Northern Asians. *Am J Phys Anthropol* 153:449–462.
16. Noback ML, Harvati K, Spoor F (2011) Climate-related variation of the human nasal cavity. *Am J Phys Anthropol* 145:599–614.
17. Yokley TR (2009) Ecogeographic variation in human nasal passages. *Am J Phys Anthropol* 138:11–22.
18. Keck T, Leiacker R, Heinrich A, Kühnemann S, Rettinger G (2000) Humidity and temperature profile in the nasal cavity. *Rhinology* 38:167–171.
19. Lindemann J, et al. (2004) A numerical simulation of intranasal air temperature during inspiration. *Laryngoscope* 114:1037–1041.
20. Williams R, Rankin N, Smith T, Galler D, Seakins P (1996) Relationship between the humidity and temperature of inspired gas and the function of the airway mucosa. *Crit Care Med* 24:1920–1929.
21. Ishikawa S, Nakayama T, Watanabe M, Matsuzawa T (2009) Flow mechanisms in the human olfactory groove: Numerical simulation of nasal physiological respiration during inspiration, expiration, and sniffing. *Arch Otolaryngol Head Neck Surg* 135:156–162.
22. Nishimura T, et al. (2016) Impaired air conditioning within the nasal cavity in flat-faced Homo. *PLoS Comput Biol* 12:e1004807.
23. Combes SA, Rundle DE, Iwasaki JM, Crall JD (2012) Linking biomechanics and ecology through predator-prey interactions: Flight performance of dragonflies and their prey. *J Exp Biol* 215:903–913.
24. Higham TE, Birn-Jeffery AV, Collins CE, Hulsey CD, Russell AP (2015) Adaptive simplification and the evolution of gecko locomotion: Morphological and biomechanical consequences of losing adhesion. *Proc Natl Acad Sci USA* 112:809–814.
25. Gómez-Valdés J, et al. (2013) Lack of support for the association between facial shape and aggression: A reappraisal based on a worldwide population genetics perspective. *PLoS One* 8:e52317.
26. Gunz P, Mitteroecker P (2013) Semilandmarks: A method for quantifying curves and surfaces. *Hystrix* 24:103–109.
27. Trouet V, Van Oldenborgh GJ (2013) KNMI climate explorer: A web-based research tool for high-resolution paleoclimatology. *Tree-Ring Res* 69:3–13.
28. Lande R (1980) The genetic covariance between characters maintained by pleiotropic mutations. *Genetics* 94:203–215.
29. Ackermann RR, Cheverud JM (2002) Discerning evolutionary processes in patterns of tamarin (genus Saguinus) craniofacial variation. *Am J Phys Anthropol* 117:260–271.
30. Rae TC, Koppe T, Stringer CB (2011) The Neanderthal face is not cold adapted. *J Hum Evol* 60:234–239.
31. Rae TC, Koppe T, Stringer CB (2011) Hyperpneumatized Neanderthals? Reply to Holton et al. (2011). *J Hum Evol* 61:628–629.
32. Paternoster L, et al. (2012) Genome-wide association study of three-dimensional facial morphology identifies a variant in PAX3 associated with nasion position. *Am J Hum Genet* 90:478–485.
33. Hallgrímsson B, et al. (2009) Deciphering the palimpsest: Studying the relationship between morphological integration and phenotypic covariation. *Evol Biol* 36:355–376.
34. Martínez-Abadías N, et al. (2011) FGF/FGFR signaling coordinates skull development by modulating magnitude of morphological integration: Evidence from Apert syndrome mouse models. *PLoS One* 6:e26425.
35. Howells WW (1989) *Skull Shapes and the Map: Craniometric Analyses in the Dispersion of Modern Homo* (Harvard Univ Press, Cambridge, MA), Vol 79, pp 1–189.
36. Schwartz JH, Tattersall I (2002) *The Human Fossil Record Volume 1. Terminology and Craniodental Morphology of Genus Homo (Europe)* (John Wiley and Sons, New York).
37. Klingenberg CP (2011) MorphoJ: An integrated software package for geometric morphometrics. *Mol Ecol Resour* 11:353–357.
38. Calvo N, Idelsohn S, Oñate E (2003) The extended Delaunay tessellation. *Eng Comput* 20:583–600.
39. Oxnard C, O'Higgins P (2009) Biology clearly needs morphometrics. Does morphometrics need biology? *Biol Theory* 4:84–97.
40. Wiley DF, et al. (2005) Evolutionary morphing. *Proceedings of the IEEE Visualization Conference* (Institute of Data Analysis and Visualization, Minneapolis), pp 431–438.

ANTHROPOLOGY

www.manaraa.com